Investigation of the Gold Nanoparticles Synthesis, Mechanism and Characterization Using the Turkevich Method

Arnaldo César Pereira *, Ana E.F. Oliveira , Mayra A. C. Resende , Lucas Franco Ferreira

Posted Date: 22 May 2023

doi: 10.20944/preprints202305.1494.v1

Keywords: Gold nanoparticles; Synthesis; Nanomaterial; Turkevich method; characterization

Article

Investigation of the Gold Nanoparticles Synthesis, Mechanism and Characterization Using the Turkevich Method

Ana Elisa F. Oliveira [1], Arnaldo C. Pereira [1,*], Mayra A. C. Resende [1] and Lucas F. Ferreira [2]

[1] Departamento de Ciências Naturais, Universidade Federal de São João del-Rei, UFSJ, São João del-Rei, MG, 36307-352, Brazil
[2] Instituto de Ciência e Tecnologia, Universidade Federal dos Vales do Jequitinhonha e Mucuri, UFVJM, Diamantina, MG, 39100-000, Brazil
* Correspondence: arnaldo@ufsj.edu.br

Abstract: The gold nanoparticle (AuNP) was synthesized using the well-known Turkevich method. This article explains didactic step-by-step of the synthesis, showing pictures of the entire process, including a well-explained mechanism and characterization study. The synthesis includes the reduction of NaAuCl4 using sodium citrate in high temperature (around 90 ^{0}C). The two main mechanisms used to explain the AuNP synthesis via Turkevich method were explained. The first mechanism considerate that a nanowire intermediary and the other proposed that aggregate intermediates are not formed at any time during the synthesis. The materials (NaAuCl4 and AuNP) were characterized by UV-Vis, SEM, AFM, XRD and DLS. The UV-Vis exhibit an absorption maximum in 521 nm because the surface plasmon resonance (SPR) absorption band of AuNP. The SEM images of NaAuCl4 presents crystals with cubic shapes, while the AuNP presents average particle size of about 16-25 nm and particles that appear mainly spherical. To confirm the particles shapes, the AFM was conducted and it was possible to observe clearly the individual spherical nanoparticles. The XRD of AuNP showed the four main characteristic peaks for silver corresponding to (111), (200), (220) and (311) planes, confirming the cubic (FCC) silver. The DLS presented the average particle size of 3.3 ± 0.9 nm and the polydispersity index (PDI) of 0.574. In summary, the AuNP was synthesized using a simple and fast method. The result was a spherical and ultrasmall particle, that can be used is several applications.

Keywords: gold nanoparticles; synthesis; nanomaterial; Turkevich method; characterization

1. Introduction

During the 1850s, Faraday fabricated gold slides and examined by shining light through them. For that purpose, he used sodium chloroaurate (NaAuCl4) with a reducing suspension such as phosphorus in carbon disulfide, where the color changed from bright yellow to deep ruby. The resulting liquid was known as "Faraday's Gold" [1-3]. While shining a beam of light through the liquid, Faraday observed that a portion of the light is scattered leading to a divergence of the light beam. That was explained by him due the presence of fine particles of gold dispersed in the liquid "in a state of extreme division", not visible in any microscopy. This behavior is known today as the Faraday-Tyndall effect. The studies of Faraday are recognized as the emergence of Nanoscience and Nanotechnology [1-3].

Since them, gold nanoparticles (AuNPs) have been fabricated in various sizes and shapes, using different techniques and routes. The AuNPs has attractive physical properties including surface plasmon resonance (SPR), the ability to quench fluorescence, the surface-enhanced Raman scattering (SERS) and redox activity. Over the last decade these properties have been used in the fabrication of electronic devices, imaging, sensing, printable inks, photodynamic therapy, therapeutic agent delivery, sensors, catalysis, probes and others [4-11].

Also, the AuNPs presents excellent biocompatibility due to the high binding affinity to biomolecules. Both covalent and noncovalent approaches have been designed to conjugate the AuNPs. The most common covalent conjugation is the direct attachment of the thiolate molecule to

Preprints (www.preprints.org) | NOT PEER-REVIEWED | Posted: 22 May 2023 doi:10.20944/preprints202305.1494.v1

AuNPs. Concerning the non-covalent, it is usually due electrostatic interactions, hydrophobic interaction and specific binding affinity [4,12].

The most common approach to synthesize AuNPs is the chemical methods. It usually employs three components: metal precursor, reducing agent and stabilizing/capping agents. The metal precursor is the metallic salt, in that case, the gold. The chemical reduction can be performed using various chemical reductants, such as sodium citrate (Na3C6H5O7), hydrazine (N2H4), ascorbic acid (HC6H7O6), sodium borohydride (NaBH4) and others (Lee et al. 2019). Also, the stabilizing agent is used to be absorbed onto the AuNP surface to avoid agglomeration. The most common are phosphorus ligands, trisodium citrate dihydrate (C6H9Na3O9), cetyltrimethylammoniumbromide (CTAB), chitosan, surfactants and others polymers [12-15].

Although there are lots of article talking about synthesis of gold nanoparticle, at the best of our knowledgement, we did not find an article that explained didactic step-by-step of the synthesis, the role of each reagent and showing pictures of the entire process, including a well-explained mechanism and characterization study. Therefore, in this work, the gold nanoparticle (AuNP) was synthesized using the well-known Turkevich method and these aspects were taken in consideration in the discussions.

2. Materials and Methods

2.1. Reagents

Sodium citrate (Na3C6H5O7) was acquired from Synth (Brazil). Sodium tetrachloroaurate(III) dehydrate (NaAuCl4) from Sigma-Aldrich (Brazil). All reagents were of analytical purity and all solutions were prepared with purified water by Millipore Milli-Q system with resistivity of 18.2 MΩ.cm (at 25°C).

2.2. Synthesis of Gold Nanoparticle

The synthesis is illustrated in Figure 1. The gold nanoparticle (AuNP) was fabricated using the classical citrate synthesis, also known as Turkevich method.

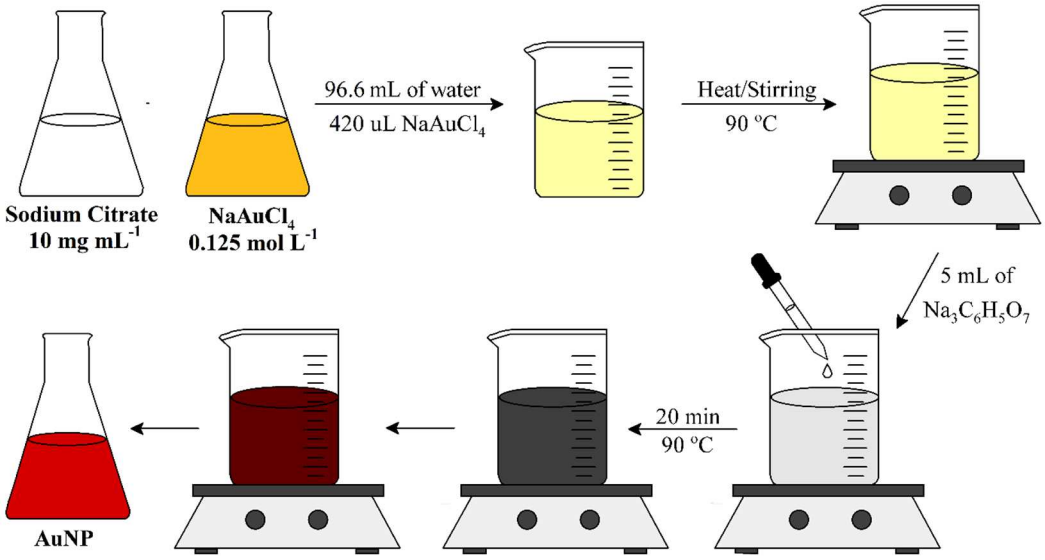

Figure 1. Schematic diagram showing the steps for gold nanoparticles (AuNP) synthesis.

Initially, stock solutions of sodium citrate 10 mg mL-1 and sodium tetrachloroaurate (NaAuCl4) 0.125 mol L-1 was prepared. Then 420 µL of NaAuCl4 was added to 94.6 mL of deionized water and the solution was maintained under agitation and heat until 90 ºC. When it achieved the required temperature, 5 mL of sodium citrate was quickly added. The agitation and heat at 90 ºC were kept for 20 minutes. The color of the suspension changed from light yellow to grey, and then to red,

 doi:10.20944/preprints202305.1494.v1

indicating the formation of gold nanoparticles (AuNP). After, the AuNP suspension was cooled slowly to room temperature and kept at 4 ^{0}C.

2.3. Characterization Techniques

The samples of $NaAuCl_4$ and AuNP were characterized using different techniques. UV-Vis Spectrometry was performed using a spectrophotometer UV-2550 from Shimadzu in 300 - 800 nm. Both samples were diluted in deionized water using a quartz cuvette.

The Scanning Electron Microscopy (SEM) images were recorded using a microscope JEOL JSM 300-LV. The measurements were performed by Prof. Dr. Lucas Franco Ferreira of Federal University of the Jequitinhonha and Mucuri Valleys (UFVJM). X-ray Diffraction analysis (XRD) were performed using a Shimadzu model XRD 6000 (30 kV 30 mA), Cu-Kα (λ = 1.54 Å) in range 30 - 90°. In both techniques (SEM and XRD) the samples of NaAuCl4 and AuNP were placed on an acetate slide and dried at 70 ^{0}C.

The Atomic Force Microscopy (AFM) characterization was carried out using the microscopy Bruker Multimode 8 (MM8). It was used scan size of 5.00 μm and amplitude 5000 mV. The AFM was conducted only for the AuNP. The sample was dried in a graphite substrate and placed on a circular metallic AFM holder using silver tape.

3. Results

3.1. Synthesis of Gold Nanoparticle

The AuNPs were synthesized using the Turkevich method and the photos of the process is presented in Figure 2(a). This classical method was presented by Turkevich in 1951 using trisodium citrate as a reducing agent. Since them, several articles have been proposed the synthesis using modified Turkevich method [16-19].

As observed in the photos, during the synthesis the color changed from pale yellow to a transparent colorless suspension almost immediately after the addition of the citrate. The suspension remained colorless for 10 seconds and it turned rapidly to bluish gray. The next minutes the suspension continued to darken into a dark blue/purple that was almost black. At this point, the suspension started to turn into deep wine red, characteristic of AuNP. Until the end of the synthesis, that reached 20 minutes, the color does not change considerably.

It is important to highlighted that the suspension has to be stirred continuously during the synthesis or agglomeration/precipitation of gold will be formed. Also, the temperature was precisely controlled, since it is a defining parameter in the synthesis of AuNP. While increasing the temperature, usually decreases the AuNP size. Hence, the temperature chosen was 90 ^{0}C and it was kept constant during all synthesis [20].

Comparing the stock solution of NaAuCl4 and the synthesized AuNP, it is clearly observed the color change, as shown in Figure 2(b). For spherical particle around 30 nm, the AuNP absorbs light in the blue-green portion of the spectrum, reflecting the red light. That results in the AuNP red suspension, characteristic of stable suspensions of gold nanoparticles. Although, as the particle size increases the absorption shifts to higher wavelight. The red light is absorbed and the blue/purple light is reflected [21]. Hence, the formation of red AuNP in the synthesis indicate that the nanoparticle was around 30 nm.

Several authors discuss about the mechanism of AuNP synthesis. In general, there is two mechanisms used to explained the Turkevich method. They both will be discussed in this topic and related to the synthesis performed in this work. The first mechanism, presented in Figure 3, considerate that an intermediary is formed during the synthesis. While the second mechanism in Figure 4 purpose that non aggregate intermediates is formed.

Preprints (www.preprints.org) | NOT PEER-REVIEWED | Posted: 22 May 2023 doi:10.20944/preprints202305.1494.v1

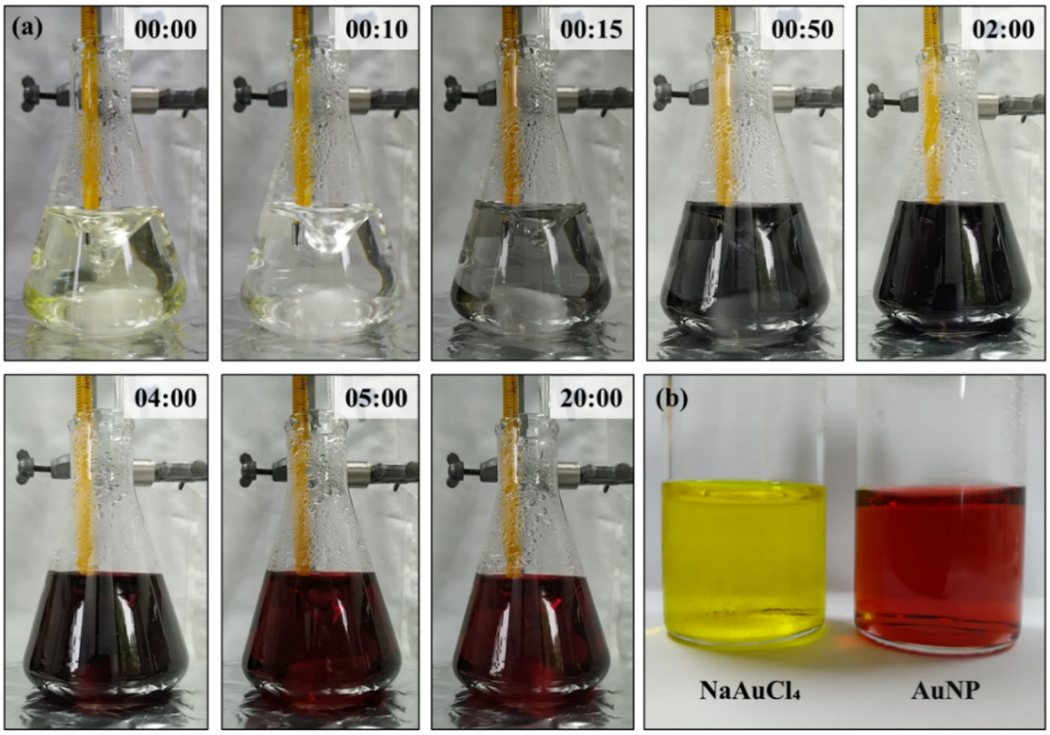

Figure 2. (a) Synthesis of gold nanoparticle (AuNP) using Turkevich method during the process; (b) Stock solution of NaAuCl4 and the synthesized AuNP after reach room temperature.

Pong et al. studied the growth mechanism in the citrate reduction of gold(III) salt and proved via transmission electron microscopy (TEM) the formation of the Au nanowire intermediate [22]. Zhao et al. also reported a formation of wire-like aggregates as an intermediate step [23].

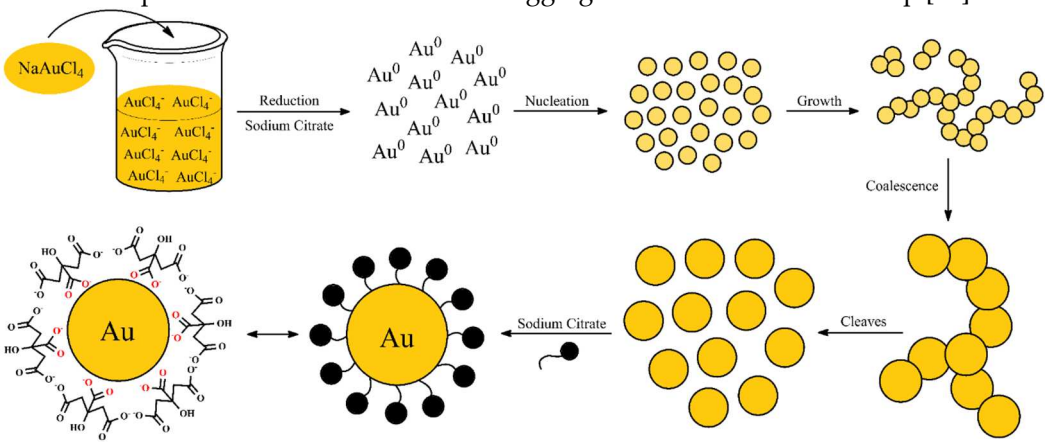

Figure 3. Schematic representation of synthesis of gold nanoparticle forming an intermediary.

Initially, the solution of NaAuCl4 is prepared in water. The pale-yellow color is due the presence of the gold salt, a yellow-gold powder. After the addition of sodium citrate, the Au3+ species were rapidly reduced to metallic gold (Au0) and it started to form small clusters. That process is observed during the colorless phase. Then the nanoclusters coalesce to form a network of nanowires turning the suspension into a bluish gray. This initial stage is extremely fast, as observed in Figure 2(a). Therefore, the color blue/purple observed during the synthesis is related to the formation of gold nanowires as an intermediate step during the AuNP growth [23-25].

As the suspensions gets darker, the diameter of the nanowires increases due to coalescence in a linear-like manner. That refers to the process where the particle merge during contact, decreasing the number of particles. At the same time, the extensive network began to cleave, leaving fragments of

Preprints (www.preprints.org) | NOT PEER-REVIEWED | Posted: 22 May 2023 doi:10.20944/preprints202305.1494.v1

spherical particles. That process is clearly observed since it gives a red color to the suspension [23-25].

However, there is another mechanism that explain the Turkevich method. Polte, et al. proposed that aggregate intermediates are not formed at any time of the Turkevich synthesis [22,26]. Wuithschick, et al. refined the theory and explained the bluish color in the middle of the synthesis [27].

The first step is the rapid reduction of NaAuCl4 by sodium citrate and the formation of small clusters. These steps occur in the first 10 seconds of the synthesis. Then the cluster grows due to coalescence, forming the citrate capped gold nanoparticles. According to Wuithschick et al. the color blue/purple observed during the synthesis is caused by the adsorption of NaAuCl4 on the nanoparticle surface influencing the surface chemistry or the dielectric constant of the surrounding medium. Therefore, after a few minutes in the synthesis, the NaAuCl4 was completely reduced resulting in the ruby red [12,18,22,26-28]

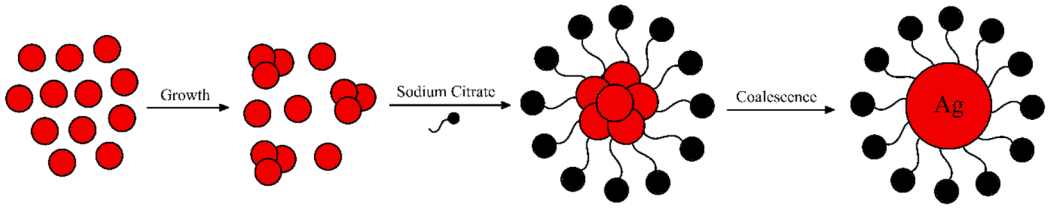

Figure 4. Schematic representation of synthesis of gold nanoparticle without intermediary.

Therefore, in this work we considerate both mechanisms proposed for the synthesis of AuNP and the perspective of different authors. That was chosen since there is no consensus among researchers concerning the mechanism.

However, both mechanism considerate the reduction of AuCl4- using citrate. Figure 5 shows the proposed mechanism involved in the reduction. As observed, the mechanism suggests two steps. First, the trivalent gold (Au3+) is reduced to monovalent gold (Au+) by citrate. While simultaneously the citrate (Cit3+) is oxidized to acetone dicarboxylate (ACDC2-). The second step involves the disproportionation reaction where metallic gold (Au0) and trivalent gold (Au3+) are produced. The overall reaction correcting the stoichiometry is also presented below in Figure 5.9 [29-32].

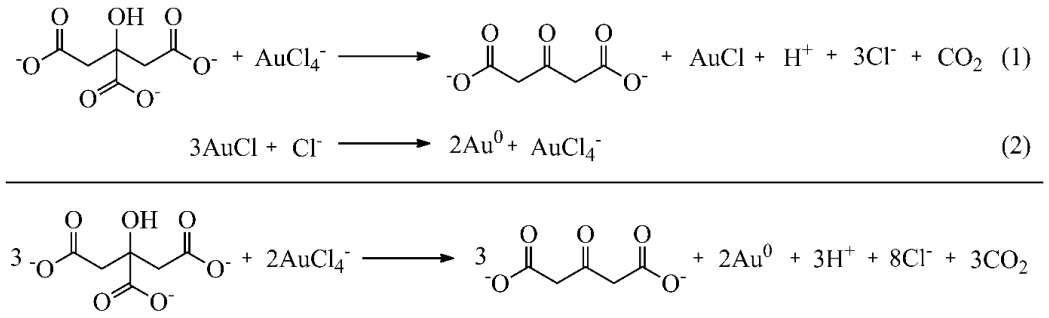

Figure 5. Accepted reduction mechanism of AuCl4- using citrate in two step redox reaction.

Past studies suggest that the acetone dicarboxylate (ACDC2-) is rapidly degraded to acetone at the synthesis temperature around 100 ºC, as shown in Figure 6. The degradation products reduce trivalent gold (Au3+) and lead to its complete conversion to Au0. Therefore, the ACDC2- acts as an auxiliary reducing agent [29,31].

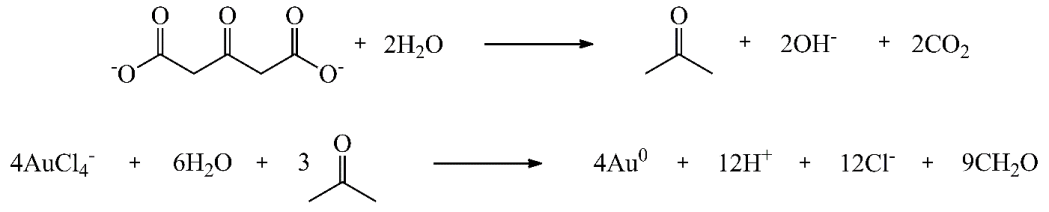

Preprints (www.preprints.org) | NOT PEER-REVIEWED | Posted: 22 May 2023 doi:10.20944/preprints202305.1494.v1

Figure 6. Decomposition of acetone dicarboxylate (ACDC2-) and reduction Au3+ by acetone.

3.2. UV-Vis Spectroscopy

Gold nanoparticles (AuNPs) exhibit a localized surface plasmon resonance (LSPR) that results in a strong absorbance band in the visible region (500 - 600 nm), that can be measured using UV-Vis spectroscopy. The spectrum obtained is presented in Figure 7. As expected, AuNP are exhibit an absorption maximum in 520 nm because the SPR absorption band [33].

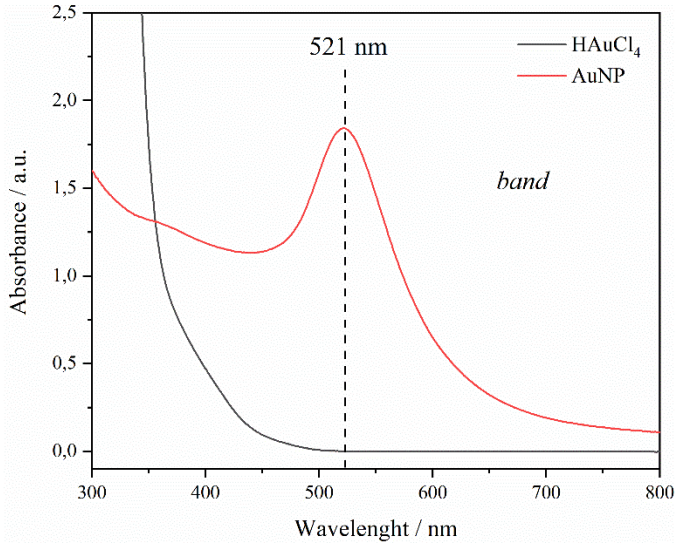

Figure 7. UV-vis absorption spectrum of sodium tetrachloroaurate and gold nanoparticles.

The surface plasmon (SP) phenomenon is the oscillations of free electrons on the solid materials surface. The surface plasmon exist in two forms: localized and propagating. The localized surface plasmon resonance (LSPR) is supported by metal nanoparticles. When the frequency of the incident light matches the natural frequency of surface electrons the LSPR occur [33,34].

The oscillating field of the incident light induce the free electrons to oscillate coherently, causing a disturbance of the electron cloud in the AuNP and leaving a portion of the particle positively charged. The electron cloud oscillates at the dipolar plasmon resonance frequency [35-37]. This phenomenon is presented in Figure 8.

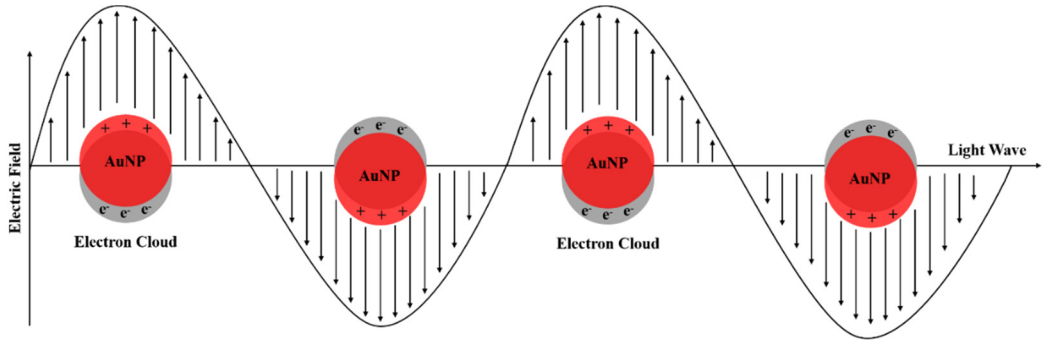

Figure 8. Schematic illustration of surface plasmon resonance (SPR) in gold nanoparticles.

The band intensity and wavelength depend on the AuNP properties including structure, shape, metal and size [33,36,38]. Typically, the surface plasmon band for spherical AuNP of 10 nm presents peaks around 520 nm in UV-Vis. As the wavelength shifts to higher values with the increasing in diameter of NPs [38]. As observed, the AuNP synthesized showed a strong broad peak at 520 nm. That result indicates the AuNP obtained has a diameter around 10 nm.

3.3. Scanning Electron Microscopy and Atomic Force Microscopy

Preprints (www.preprints.org) | NOT PEER-REVIEWED | Posted: 22 May 2023 doi:10.20944/preprints202305.1494.v1

The Scanning Electron Microscopy (SEM) technique is a valuable tool for examining the surfaces of materials [39]. In this work the SEM is used to confirm the production of AuNPs and to study the topography of the NaAuCl4 and the obtained AuNP. The images were viewed at different magnifications of 2,000X and 30,000X. The obtained images are presented in Figure 9. As observed, the images of tetrachloroaurate(III) dehydrate (NaAuCl4) presents crystals with cubic shapes. At magnification of 30,000X there is two crystals of 0.38 μm and 0.67 μm [40,41].

The SEM results revealed that the gold nanoparticles structures. The image shows a uniform distribution of AuNPs, but the surface indicates some degree of aggregation, generating random aggregates with several sizes and irregular shapes. Also, in a high magnification image, it is observed the formation of larger particles and more agglomerations [42-43]. The present average particle size could not be measured.

The image also shows particles that appear to be mainly spherical [44-46]. However, due to the limited resolution of SEM the clear shape and size of the obtained AuNPs could not be observed. Therefore, the morphology of the AuNP were also characterized with atomic force microscopy (AFM).

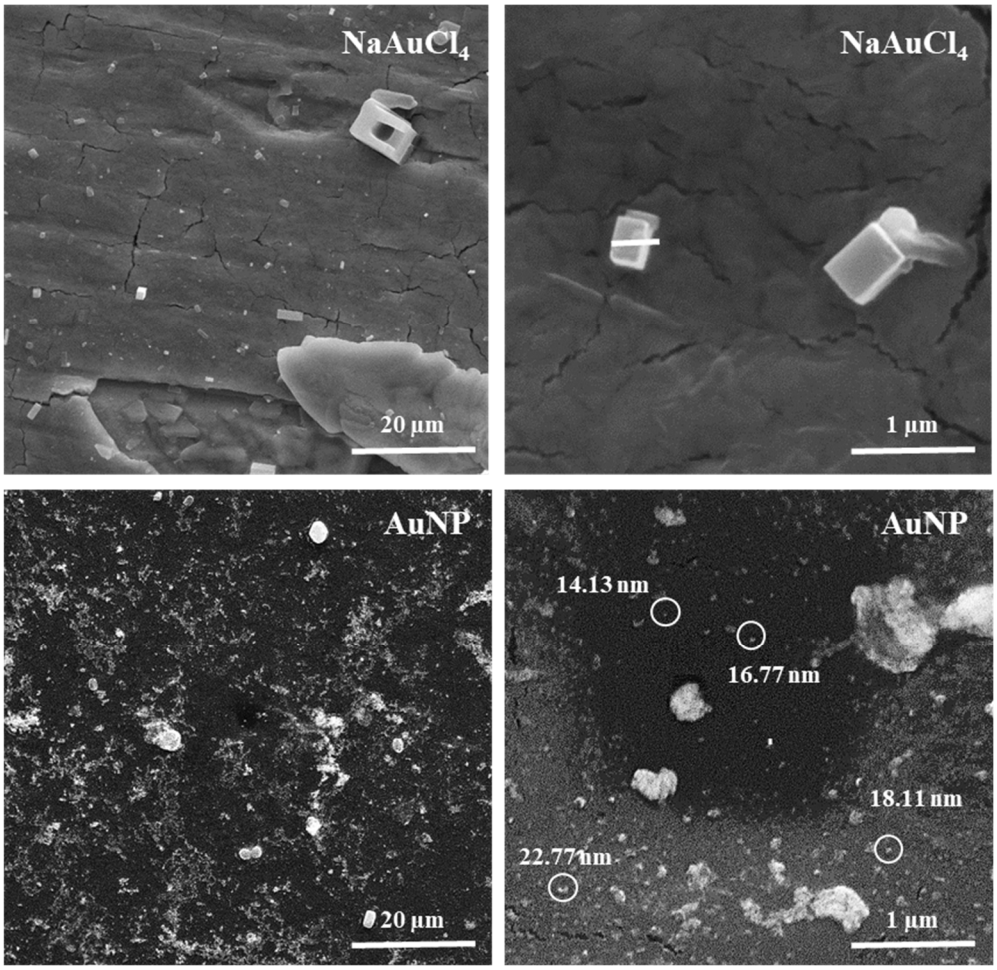

Figure 9. SEM images at 2000X and 30000X magnification of NaAuCl4 and AuNP samples.

Atomic Force Microscopy (AFM) is a powerful technique to investigate the surface morphology. The AFM scans the sample surface with a sharp tip producing a three-dimensional topography. That provides a higher level of detail for these surface [47]. The obtained images are presented in Figure 10. In the images it is possible to observe clearly the individual spherical nanoparticles and their aggregates. The average diameter of these AuNPs measured by the image was around 11 - 19 nm [48,49].

Preprints (www.preprints.org) | NOT PEER-REVIEWED | Posted: 22 May 2023 doi:10.20944/preprints202305.1494.v1

The results are in agreement with the SEM images. The size is near to the ones observed in SEM and it is possible to observe the shape more evidently. That indicates the effective synthesis of AuNP from the precursor NaAuCl4 [46]. It also shows that the particles have spherical shape with an average diameter of approximately ~15 nm.

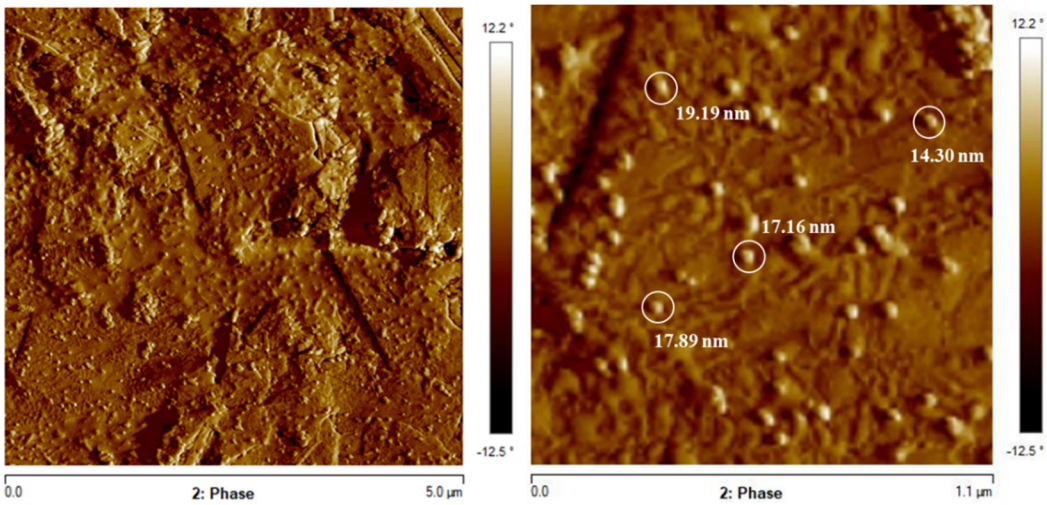

Figure 10. AFM phase images of AuNP on a bare graphite substrate. The circled regions exhibited gold nanoparticles and their diameter (particles around 11 - 19 nm).

3.4. X-Ray Diffraction Analysis

The crystallinity of synthesized AuNPs was investigated using X-ray diffraction (XRD) technique. The corresponding XRD patterns were shown in Figure 11(a). The typical XRD of NaAuCl4 exhibits several sharp intense crystalline peaks [50,51]. As expected, the diffractogram obtained showed that behavior.

The AuNP pattern exhibited four distinct peaks at 38.24^0, 44.47^0, 64.71^0 and 77.79^0. All the peaks corresponded to standard Bragg reflections (111), (200), (220) and (311) sets of lattice planes indexed to their face-centered cubic (FCC) structure [52,53]. There is another intense unassigned peak at 53.17^0 that might have resulted from some organic compound in the nanoparticle during the synthesis such as sodium citrate. However, the presence of these external peak did not alter the Bragg reflection peaks of AuNP [54,55]. The XRD results provides strong evidence confirming the synthesis of AuNP from NaAuCl4.

It is possible to measure the crystallite size of the AuNP from X-ray diffraction using the Scherrer equation, in Figure 11(b). Where D is the average crystallite size; λ is the x-ray wavelength CuK α (0.15406 nm); β is the line broadening at the full width of the peak (FWHM) in radians; θ is the Braggs angle in degrees (half of the 2θ). The Scherrer constant K depends on the how the width is determined, the shape of the crystal and size distribution. Langford and Wilson discussed the value of K in function of the crystal shape [56]. Based in this word, several authors have been used the K value of 0.94 for spherical crystals with cubic symmetry [57]. The crystallite size was calculated for all the four peaks and the results are presented in Figure 11(c). The average crystallite size obtained was 7.14 nm.

Generally, the peak width varies inversely with crystallite size. Therefore, when crystallite size increases, diffraction peak broadening decreases. However, there is others parameters that affect the result. The value obtained using the Scherrer equation is limited due the instrument, structural defects, the relationship between signal and sample and noise. So it is difficult to distinguish the broadening due to the crystallite size from others factors [58,59]. Although, the Scherrer equation provides an average value for the nanoparticle size.

Preprints (www.preprints.org) | NOT PEER-REVIEWED | Posted: 22 May 2023 doi:10.20944/preprints202305.1494.v1

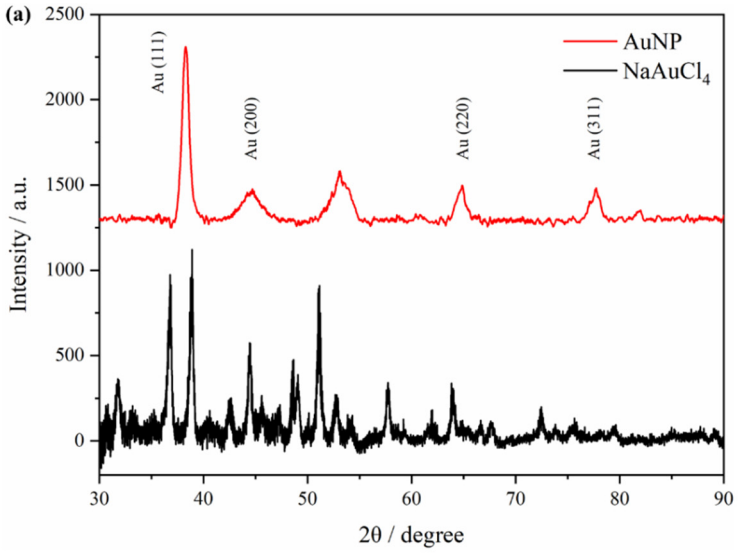

(b)

$$D = \frac{k.\lambda}{\beta.\cos\theta}$$

(c)

Peak	1	2	3	4	Average
Size / nm	11.5043	3.6358	6.6113	6.8101	7.14 ± 2.81

Figure 11. (a) XRD pattern of gold nanoparticle (AuNP) and sodium tetrachloroaurate (NaAuCl4); (b) Scherrer equation; (c) Crystallite size obtained from each peak.

3.5. Dynamic Light Scattering

The Dynamic Light Scattering (DLS) technique was used in order to evaluate the average size, size distribution and possible aggregation of the synthesized AuNPs [60,61]. The zeta potential was also measured. Figure 12 shows the graph of particle size distribution (differential number % and cumulative number %). The values obtained from the zeta potential graphs is also presented. As observed, from the particle size distribution graph, it is obtained the average particle size of 3.3 ± 0.9 nm and the polydispersity index (PDI) of 0.574. About the zeta potential, the value found was -2.33 mV.

As discussed previously, AuNPs are small gold particles with a diameter of 1 - 100 nm. Particle smaller than 10 nm can be consider ultrasmall AuNPs The particle size obtained was 3.3 ± 0.9 nm. Hence, according to the DLS the synthesized AuNP is a ultrasmall nanoparticle [62-64]. Also, in the graph only one peak is observed, indicating that there is no presence of particles of very different sizes in the as colloid [65].

The PDI describe the degree of "non-uniformity" of a distribution. The value is calculated from the width of the size distribution. The range is from 0.0 (a perfect uniform sample) to 1.0 (highly polydisperse sample with multiple particle size) [60]. PDI values above 0.7 indicates a broad particle size distribution profile [66,67]. The PDI of 0.574 obtained has a wide particle size distribution and can be considered a medium polydispersity, an acceptable value indicating moderated homogeneity.

When particles are present in a liquid, an electrical double layer (EDL) is usually formed, consisting of ions in the liquid, as presented in Figure 5.16(b). This model explains how the electrical repulsive force operates. The EDL surface is formed by two layers. The inner layer, called stern layer, is composed of opposite charged particles coupled to the core of the central particle. The outer layer, called diffuse layer, is where the ions are diffused more freely around the particle [68-70]. The double-layer properties can directly influence the zeta potential of the system. The zeta potential, or ζ potential, is the potential measured at the slipping plane: the difference between the EDL and the layer of dispersant around them [66,71].

Preprints (www.preprints.org) | NOT PEER-REVIEWED | Posted: 22 May 2023 doi:10.20944/preprints202305.1494.v1

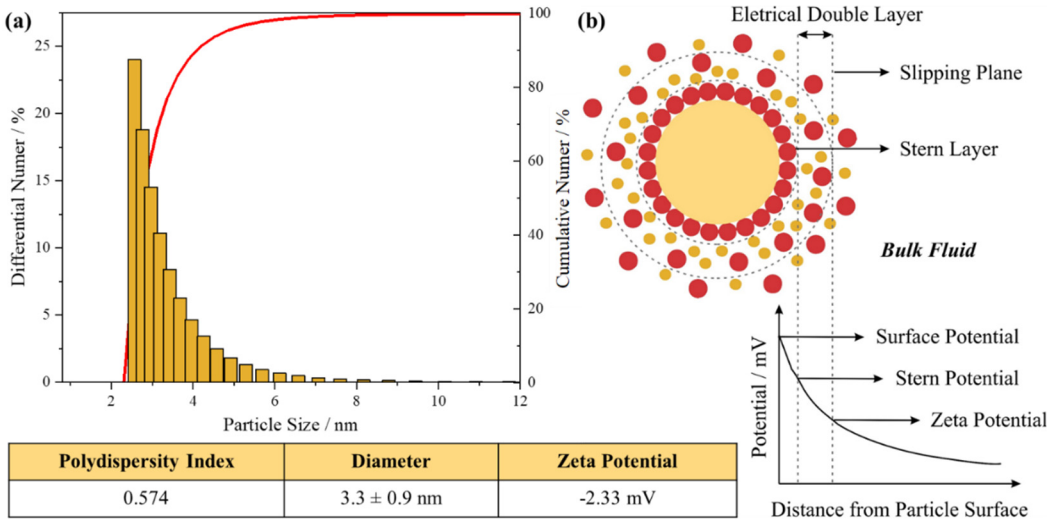

Polydispersity Index	Diameter	Zeta Potential
0.574	3.3 ± 0.9 nm	-2.33 mV

Figure 12. (a) DLS analysis of particle size distribution and zeta potential; (b) Schematic representation of the double layer that surrounds the nanoparticle in aqueous medium.

The (ZP) is an important parameter that directly affects the stability of nanodispersions [72]. Hence, it can provide a good prediction of dispersions stability. High potentials (negative or positive) are electrically stabilized, generally the repulsive forces exceed attractive forces resulting in a stable system. While low potentials tend to coagulate or flocculate [65,73]. Usually, particles with ZP in the range of -30 mV to +30 mV is considered normally stable [66].

The ZP of the synthesized AuNPs obtained, -2.33 mV, was a little small gave a slightly negative surface charge. That results can suggest that the nanoparticles may be close to the threshold of agglomeration. However, the average particle size found was very small (3.3 ± 0.9 nm), that can be an indicative that large aggregations are not observed. In theory, the zeta potential is not related to the particle size. But some author observed a relation between these two values. According to the Nakutuka et al. the absolute negative value of zeta potential of small particles is greater than that of large particles [74,75]. Since usually the smaller the nanoparticles, the easier they are to aggregate [76].

Others authors also exhibited a correlation between those values [77,78]. Another important thing to understand, is that the zeta potential is not a direct measurement of the stability, but a guide of the stability or instability of a system. Therefore, the value close to zero does not mean that the nanoparticle will absolutely become unstable and aggregate or collapse [79].

4. Conclusions

In this chapter the AuNP was synthesized using the Turkevich method. The process includes the reduction of NaAuCl4 using sodium citrate in high temperature. The result was a red suspension, that indicates the formation of a gold nanoparticle.

Two main mechanisms are used to explain the AuNP synthesis via Turkevich method. The first mechanism considerate that a nanowire intermediary is formed during the synthesis that coalescence in a linear-like manner and then cleave leaving fragments of spherical particles.

However, there is another mechanism that proposed that aggregate intermediates are not formed at any time of the Turkevich synthesis. It includes the reduction of NaAuCl4 and formation of small clusters that grows due to coalescence, forming the citrate capped gold nanoparticles.

The materials were characterized by UV-Vis, SEM, AFM. XRD and DLS. The UV-Vis spectroscopy exhibits an absorption maximum in 520 nm. That peak is characteristic of AuNP and is associated with the SPR absorption band, the oscillations of free electrons phenomenon.

The SEM images shows crystals with cubic shapes in the NaAuCl4 sample. The AuNP presented a uniform distribution with some degree of aggregation, generating random aggregates with several sizes and irregular shapes. The clear shape of the obtained AuNPs could not be observed using SEM.

Therefore, the synthesized AuNP were also characterized by AFM. Where it was possible to observe clearly the individual spherical nanoparticles, their aggregates and the average diameter of these AuNPs around 12 - 19 nm.

The typical XRD of NaAuCl4 exhibits several sharp intense crystalline peaks. While the AuNP diffractogram exhibited four characteristic peaks associated to the (111), (200), (220) and (311) crystallographic planes indexed to their face-centered cubic (FCC) structure. Then the average crystallite size was calculated using the Scherrer equation resulting in 7.14 nm. The DLS presented the average particle size of 3.3 ± 0.9 nm and the polydispersity index (PDI) of 0.574. About the zeta potential, the value found was -2.33 mV.

Comparing the results of each characterization, the AFM presented size around 11 - 19 nm, while in the DLS was 3.3 nm. Using the Scherrer equation the average crystallite size was 7.14 nm. Each technique has their own limitations, although all the techniques show nanoparticles with less than 19 nm. In summary, the AuNP was synthesized using a simple and fast method. The result was a spherical and small particle, that can be used is several applications. In this work, the AuNP will be used to modified an electrochemical sensor.

In summary, the AuNP synthesized using a simple and fast method. The result was a spherical and small particle, that can be used is several applications.

Author Contributions: Conceptualization, A.E.F.O. and A.C.P.; methodology, A.E.F.O. and M.A.C.R.; investigation, A.E.F.O., M.A.C.R. and L.F.F.; writing—original draft preparation, A.E.F.O. and M.A.C.R.; writing—review and editing, A.C.P and L.F.F.; supervision, project administration and funding acquisition A.C.P. All authors have read and agreed to the published version of the manuscript.

Funding: This research was funded by Fundação de Amparo a Pesquisa do Estado de Minas Gerais – FAPEMIG (CEX - APQ-0067-22), Conselho Nacional de Desenvolvimento Científico e Tecnológico -CNPq (40210/2021–0 and 305360/2022-1) and INCT-DATREM (465571/2014–0). This study was financed in part by the Coordenação de Aperfeiçoamento de Pessoal de Nível Superior - Brasil (CAPES) - Finance Code 001.

Data Availability Statement: Data sharing not applicable.

Conflicts of Interest: The authors declare no conflict of interest.

References

1. Heiligtag, F. J.; Niederberger, M. The fascinating world of nanoparticle research. Materials Today, 2013, 16, 262-271.
2. Edwards, P. P.; Thomas, J. M. Gold in a metallic divided state--from Faraday to present-day nanoscience. Angew Chem Int Ed Engl., 2007, 46, 5480-5486.
3. Tweney, R. D. Discovering Discovery: How Faraday Found the First Metallic Colloid. Perspectives on Science, 2006, 14, 97-121.
4. Yeh, Y. C.; Creran, B.; Rotello, V. M. Gold nanoparticles: preparation, properties, and applications in bionanotechnology. Nanoscale, 2012, 4, 1871-1880.
5. Swierczewska, M.; Lee, S.; Chen, X. The design and application of fluorophore-gold nanoparticle activatable probes. Phys. Chem. Chem. Phys., 2011, 13, 9929-9941.
6. Samanta, A.; Maiti, K. K.; Soh, K-S; Liao, X.; Vendrell, M.; Dinish, U. S.; Yun, S-W; Bhuvaneswari, R.; Kim, H.; Rautela, S.; Chung, J.; Olivo, M.; Chang, Y-T. Ultrasensitive near-infrared Raman reporters for SERS-based in vivo cancer detection. Angew. Chem. Int. Edit., 2011, 50, 6089-6092.
7. Van de Broek, B.; Devoogdt, N.; D'Hollander, A.; Gijs, H-L.; Jans, K.; Lagae, L; Muyldermans, S.; Maes, G.; Borghs, G. Specific cell targeting with nanobody conjugated branched gold nanoparticles for photothermal therapy. ACS Nano, 2011, 5, 4319-4328.
8. Liang, T. C.; Lin, H. C. Supramolecular assembly of H-bonded copolymers/complexes/nanocomposites and fluorescence quenching effects of surface-modified gold nanoparticles on fluorescent copolymers containing pyridyl H-acceptors and acid H-donors. J. Mater. Chem., 2009, 19, 4753-4763.
9. Lou, T.; Wang, Y.; Li, J.; Peng, H.; Xiong, H.; Chen, L. Rapid detection of melamine with 4-mercaptopyridine-modified gold nanoparticles by surface-enhanced Raman scattering. Anal. Bioanal. Chem., 2011, 401, 333-338.
10. Li, X.; Wang, J.; Sun, L.; Wang, Z. Gold nanoparticle-based colorimetric assay for selective detection of aluminium cation on living cellular surfaces. Chem. Commun., 2010, 46, 988-990.
11. Kumar, S. S.; Kwak, K.; Lee, D. Electrochemical sensing using quantum-sized gold nanoparticles. Anal. Chem., 2011, 83, 3244-3247.

12. Souza, C. D.; Nogueira, B. R.; Rostelato, M. E. C. M. Review of the methodologies used in the synthesis gold nanoparticles by chemical reduction. Journal of Alloys and Compounds, 2019, 798, 714-740.
13. Zhang, X.-F.; Liu, Z.-G.; Shen, W.; Gurunathan, S. Silver Nanoparticles: Synthesis, Characterization, Properties, Applications, and Therapeutic Approaches. Int J Mol Sci., 2016, 17, 1534.
14. Zhao, P.; Li, N.; Astruc, D. State of the art in gold nanoparticle synthesis. Coord. Chem. Rev., 2013, 257, 638-665.
15. Chanda, N.; Kan, P.; Watkinson, L. D.; Shukla, R.; Zambre, A.; Carmack, T. L.; Engelbrecht, H.; Lever, J. R.; Katti, K.; Fent, G. M.; Casteel, S. W.; Smith, C. J.; Miller, W. H.; Jurisson, S.; Boote, E.; Robertson, J. D.; Cutler, C.; Dobrovolskaia, M.; Kannan, R.; Katti, K. V. Radioactive gold nanoparticles in cancer therapy: therapeutic efficacy studies of GA-198AuNP nanoconstruct in prostate tumor-bearing mice. Nanomed. Nanotechnol. Biol. Med., 2010, 6, 201-209.
16. Dobrowolska, P.; Krajewska, A.; Gajda-R?czka, M.; Bartosewicz, B.; Nyga, P.; Jankiewicz, B. Application of Turkevich Method for Gold Nanoparticles Synthesis to Fabrication of SiO2@Au and TiO2@Au Core-Shell Nanostructures. Materials, 2015, 8, 2849-2862.
17. Nirala, N. R.; Saxena, P. S.; Srivastava, A. Colorimetric detection of cholesterolbased on enzyme modified gold nanoparticles. Spectrochim. Acta Part A Mol.Biomol. Spectrosc., 2018, 190, 506-512.
18. Polte, J. Fundamental growth principles of colloidal metal nanoparticles - a new perspective. CrystEngComm, 2015, 17, 6809-6830.
19. Shi, D.; Sheng, F.; Zhang, X.; Wang, G. Gold nanoparticle aggregation: colori-metric detection of the interactions between avidin and biotin, Talanta, 2018, 185, 106-112.
20. Tran, M.; DePenning, R.; Turner, M.; Padalkar, S. Effect of citrate ratio and temperature on gold nanoparticle size and morphology. Mater. Res. Express, 2016, 3, 105027.
21. Montazer, M.; Harifi, T. Chapter 2 - Nanofinishing: Fundamental principles. In The Textile Institute Book Series - Nanofinishing of Textile Materials. Woodhead Publishing, 2018, pp. 19-34.
22. Polte, J.; Tuaev, X.; Wuithschick, M.; Fischer, A.; Thuenemann, A. F.; Rademann, K.; Karehnert, R.; Emmerling, F. Formation Mechanism of Colloidal Silver Nanoparticles: Analogies and Differences to the Growth of Gold Nanoparticles. ACS Nano, 2012a, 6, 5791-5802.
23. Zhao, L.; Jiang, D.; Cai, Y.; Ji, X.; Xie, R.; Yang, W. Tuning the Size of Gold Nanoparticles in the Citrate Reduction by Chloride Ions. Nanoscale, 2012, 4, 5071-5076.
24. Pong, B.-K.; Elim, H. I.; Chong, J.-X.; Ji, W.; Trout, B. L.; Lee, J.-Y. New Insights on the Nanoparticle Growth Mechanism in the Citrate Reduction of Gold(III) Salt:? Formation of the Au Nanowire Intermediate and Its Nonlinear Optical Properties. The Journal of Physical Chemistry C, 2007, 111, 6281-6287.
25. Ji, X.; Song, X.; Li, J.; Bai, Y.; Yang, W.; Peng, X. Size Control of Gold Nanocrystals in Citrate Reduction: The Third Role of Citrate. J. Am. Chem. Soc., 2007, 129, 13939-13948.
26. Polte, J.; Erler, R.; Thünemann, A. F.; Sokolov, S.; Ahner, T. T.; Rademann, K.; Kraehnert, R. Nucleation and Growth of Gold Nanoparticles Studied via in situ Small Angle X-ray Scattering at Millisecond Time Resolution. ACS Nano, 2012b, 4, 1076-1082.
27. Wuithschick, M.; Birnbaum, A.; Witte, S.; Sztucki, M.; Vainio, U.; Pinna, N.; Polte, J. Turkevich in New Robes: Key Questions Answered for the Most Common Gold Nanoparticle Synthesis. ACS Nano, 2015, 9, 7052-7071.
28. Badilescu, S.; Packirisamy, M. Microfluidics-Nano-Integration for Synthesis and Sensing. Polymers, 2012, 4, 1278-1310.
29. Gao, Y.; Torrente-Murciano, L. Mechanistic insights of the reduction of gold salts in the Turkevich protocol. Nanoscale, 2020, 12, 2740-2751.
30. Heinzerling, P.; Oetken, M. Nanochemistry - A Split between 18th Century and Modern Times. World Journal of Chemical Education, 2018, 6, 1-7.
31. Leng, W.; Pati, P.; Vikesland, J. Room temperature seed mediated growth of gold nanoparticles: mechanistic investigations and life cycle assessment. Environ. Sci.: Nano, 2015, 2, 440-453.
32. Kumar, S.; Gandhi, K. S.; Kumar, R. Modeling of Formation of Gold Nanoparticles by Citrate Method. Industrial & Engineering Chemistry Research, 2007, 46, 3128-3136.
33. Jana, J.; Ganguly, M.; Pal, T. Enlightening surface plasmon resonance effect of metal nanoparticles for practical spectroscopic application. RSC Advances, 2016, 6, 86174-86211.
34. Sadrolhosseini, A. R.; Noor, A. S. M.; Moksin, M. M. Application of Surface Plasmon Resonance Based on a Metal Nanoparticle. In Plasmonics - Principles and Applications; IntechOpen, 2012, pp. 253-282.
35. Umashankari, J.; Inbakandan, D.; Ajithkumar, T.; Balasubramanian, T. Mangrove plant, Rhizophora mucronata (Lamk, 1804) mediated one pot green synthesis of silver nanoparticles and its antibacterial activity against aquatic pathogens. Saline Systems, 2012, 8, 11-19.
36. Sevenler, D.; Ünlü, N. L.; Ünlü, M. S. Nanoparticle Biosensing with Interferometric Reflectance Imaging. Nanobiosensors and Nanobioanalyses, 2015, 1, 81-95.

37. Waghmode, S.; Chavan, P.; Kalyankar, V.; Dagade, S. Synthesis of Silver Nanoparticles Using Triticum aestivum and its Effect on Peroxide Catalytic Activity and Toxicology. Journal of Chemistry, 2013, 265864, 1-5.
38. Thomas, K. G. Surface Plasmon Resonances in Nanostructured Materials. Nanomaterials Chemistry, 2007, 6, 185-218.
39. Pereira-da-Silva, M. A.; Ferri, F. A. Scanning Electron Microscopy. Nanocharacterization Techniques, 2017, 1, 1-35.
40. Ali, M. A.; Ali, M. F.; Ciliberto, E.; Greco, E.; Mello, D.; Viscuso, E. A new method for the preparation of gelatin nanolayer: a possible approach to the in situ consolidation of damaged gelatin photographic emulsions. Applied Physics A, 122, 2016, 1-15.
41. Chen, Y.; Gu, X.; Nie, C.-G.; Jiang, Z.-Y.; Xie, Z.-X.; Lin, C.-J. Shape controlled growth of gold nanoparticles by a solution synthesis. Chemical Communications, 2005, 33, 4181-4183.
42. Benson, J.; Fung, C. M.; Lloyd, J. S.; Deganello, D.; Smith, N. A.; Teng, K. S. Direct patterning of gold nanoparticles using flexographic printing for biosensing applications. Nanoscale Research Letters, 2015, 10, 127.
43. Devi, R. A.; Francis, A. P.; Devasena, T. Green-synthesized gold nanocubes functionalized with bisdemethoxycurcumin analog as an ideal anticancer candidate. Green Processing and Synthesis, 2014, 3, 47-61.
44. Çulha, M.; Kahraman, M.; Tokman, N.; Türko?lu, G. Surface-Enhanced Raman Scattering on Aggregates of Silver Nanoparticles with Definite Size. The Journal of Physical Chemistry C, 2008, 112, 10338-10343.
45. Rajeshkumar, S.; Malarkodi, C. In Vitro Antibacterial Activity and Mechanism of Silver Nanoparticles against Foodborne Pathogens. Bioinorganic Chemistry and Applications, 2014, 581890, 1-10.
46. Platnich, C. M.; Banerjee, A.; Kollath, V. O.; Karan, K.; Trudel, S. Thiol-ene click microcontact printing of gold nanoparticles onto silicon surfaces. Canadian Journal of Chemistry, 2018, 96, 190-195.
47. Novotna, V.; Horak, J.; Konecny, M.; Hegrova, V.; Novotny, O.; Novacek, Z.; Neuman, J. AFM-in-SEM as a Tool for Comprehensive Sample Surface Analysis. Microscopy Today, 2020, 28, 38-46.
48. Brobbey, K. J.; Haapanen, J.; Mäkelä, J. M.; Gunell, M.; Eerola, E.; Rosqvist, E.; Toivakka, M. Characterization of flame coated nanoparticle surfaces with antibacterial properties and the heat-induced embedding in thermoplastic-coated paper. SN Applied Sciences, 2018, 1, 65-79.
49. Darwich, S.; Mougin, K.; Rao, A.; Gnecco, E.; Jayaraman, S.; Haidara, H. Manipulation of gold colloidal nanoparticles with atomic force microscopy in dynamic mode: influence of particle-substrate chemistry and morphology, and of operating conditions. Beilstein Journal of Nanotechnology, 2011, 2, 85-98.
50. Novais, A. L. F.; Lima, A. P. P.; Santos, A. R. S.; Bezerra, R. R. R. Ferreira, F. C. L.; Souza, D. N. Caracterização estrutural e morfológica de compostos químicos para produção vítrea. Scientia Plena, 2019, 15, 074810.
51. Aziz, S. B.; Abdulwahid, R. T.; Rasheed, M. A.; Abdullah, O. G.; Ahmed, H. M. Polymer Blending as a Novel Approach for Tuning the SPR Peaks of Silver Nanoparticles. Polymers, 2017, 9, 48-60.
52. Milaneze, B. A.; Oliveira, J. P.; Augusto, I.; Keijok, W. J.; Côrrea, A. S.; Ferreira, D. M.; Guimarães, M. C. C. Facile Synthesis of Monodisperse Gold Nanocrystals Using Virola oleifera. Nanoscale Research Letters, 2016, 11, 465-472.
53. Krishnamurthy, S.; Esterle, A.; Sharma, N. C.; Sahi, S. V. Yucca-derived synthesis of gold nanomaterial and their catalytic potential. Nanoscale Res Lett, 2014, 9, 627-637.
54. Nejad, M. S.; Bonjar, G. H. S.; Khaleghi N. Biosynthesis of gold nanoparticles using streptomyces fulvissimus isolate. Nanomed J, 2015, 2, 153-159.
55. Singh, M.; Kalaivani, R.; Manikandan, S.; Sangeetha, N.; Kumaraguru, A. K. Facile green synthesis of variable metallic gold nanoparticle using Padina gymnospora, a brown marine macroalga. Applied Nanoscience, 2012, 3, 145-151.
56. Langford, J. I.; Wilson, A. J. C. Scherrer after sixty years: A survey and some new results in the determination of crystallite size. Journal of Applied Crystallography, 1978, 11, 102-113.
57. Ingham, B.; Toney, M. F. X-ray diffraction for characterizing metallic films. Metallic Films for Electronic, Optical and Magnetic Applications, 2014, 1, 3-38.
58. Miranda, M. A. R.; Sasaki, J. M. The limit of application of the Scherrer equation. Acta Crystallographica Section A Foundations and Advances, 2018, 74, 54-65.
59. Rabiei, M.; Palevicius, A.; Monshi, A.; Nasiri, S.; Vilkauskas, A.; Janusas, G. Comparing Methods for Calculating Nano Crystal Size of Natural Hydroxyapatite Using X-Ray Diffraction. Nanomaterials, 2020, 10, 1627-1648.
60. Danaei, M.; Dehghankhold, M.; Ataei, S.; Hasanzadeh Davarani, F.; Javanmard, R.; Dokhani, A.; Mozafari, M. Impact of Particle Size and Polydispersity Index on the Clinical Applications of Lipidic Nanocarrier Systems. Pharmaceutics, 2018, 10, 57.

61. Gao, Y.; Anand, A. V. M.; Ramachandran, V.; Karthikkumar, V.; Shalini, V.; Vijayalakshmi, S.; Ernest, D. Biofabrication of Zinc Oxide Nanoparticles from Aspergillus niger, Their Antioxidant, Antimicrobial and Anticancer Activity. Journal of Cluster Science, 2019, 1, 1-10.
62. Kathiravan, G.; Yamini, K. R.; Rajagopal, K.; Sambandam, A. Phytogenic Synthesis of Nano Silver from Madagascar Periwinkle Extracts and Their Angiogenic Activities in Zebrafish Embryos (ZFE). Nanoscience and Nanotechnology Letters, 2020, 12, 79-87.
63. Gontijo, L. A. P.; Raphael, E.; Ferrari, D. P. S.; Ferrai, J. L.; Lyon, J. P.; Schiavon, M. A. pH effect on the synthesis of different size silver nanoparticles evaluated by DLS and their size-dependent antimicrobial activity. Matéria (Rio J.), 2020, 25, 4.
64. Zarschler, K.; Rocks, L.; Licciardello, N.; Boselli, L.; Polo, E.; Garcia, K. P.; Dawson, K. A. Ultrasmall inorganic nanoparticles: State-of-the-art and perspectives for biomedical applications. Nanomedicine: Nanotechnology, Biology and Medicine, 2016, 12, 1663-1701.
65. Banerjee, S.; Saha, A. K.; Show, B.; Ganguly, J.; Bhattacharyay, R.; Datta, S. K.; Mukherjee, N. A regular rippled pattern formed by the molecular self-organization of polyvinylpyrrolidone encapsulated Ag nanoparticles: a high transmissive coating for efficiency enhancement of c-Si solar cells. RSC Advances, 2015, 5, 5667-5673.
66. Joseph, E.; Singhvi, G. Multifunctional nanocrystals for cancer therapy: a potential nanocarrier. Nanomaterials for Drug Delivery and Therapy, 2019, 1, 91-116.
67. Mudalige, T.; Qu, H.; Van Haute, D.; Ansar, S. M.; Paredes, A.; Ingle, T. Characterization of Nanomaterials. Nanomaterials for Food Applications, 2019, 1, 313-353.
68. Nisticò, R.; Cesano, F.; Garello, F. Magnetic Materials and Systems: Domain Structure Visualization and Other Characterization Techniques for the Application in the Materials Science and Biomedicine. Inorganics, 2020, 8, 6.
69. Park, S.-J.; Seo, M.-K. Intermolecular Force. Interface Science and Technology, 2011, 1, 1-57.
70. Carvalho, P. M.; Felício, M. R.; Santos, N. C.; Gonçalves, S.; Domingues, M. M. Application of Light Scattering Techniques to Nanoparticle Characterization and Development. Frontiers in Chemistry, 2018, 6, 1-17.
71. Adegoke, O.; Park, E. Y. Gold Nanoparticle-Quantum Dot Fluorescent Nanohybrid: Application for Localized Surface Plasmon Resonance-induced Molecular Beacon Ultrasensitive DNA Detection. Nanoscale Research Letters, 2016, 11, 523
72. Ding, Z.; Jiang, Y.; Liu, X. Nanemulsions-Based Drug Delivery for Brain Tumors. Nanotechnology-Based Targeted Drug Delivery Systems for Brain Tumors, 2018, 1, 327-358.
73. Lu, G. W.; Gao, P. Emulsions and Microemulsions for Topical and Transdermal Drug Delivery. Handbook of Non-Invasive Drug Delivery Systems, 2010, 1, 59-94.
74. Nakatuka, Y.; Yoshida, H.; Fukui, K.; Matuzawa, M. The effect of particle size distribution on effective zeta-potential by use of the sedimentation method. Advanced Powder Technology, 2015, 26, 650-656.
75. Zuki, N. M.; Ismail, N.; Omar, F. M. Evaluation of zeta potential and particle size measurements of multiple coagulants in semiconductor wastewater. 6th International Conference on Environment (ICENV2018), 2019, 1, 1-10.
76. Wang, N.; Cheng, X.; Li, N.; Wang, H.; Chen, H. Nanocarriers and Their Loading Strategies. Advanced Healthcare Materials, 2018, 1, 1801002.
77. Kazi, S. N.; Badarudin, A.; Zubir, M. N. M.; Ming, H. N.; Misran, M.; Sadeghinezhad, E.; Syuhada, N. I. Investigation on the use of graphene oxide as novel surfactant to stabilize weakly charged graphene nanoplatelets. Nanoscale Research Letters, 2015, 10, 1-15.
78. Choudhari, Y. M.; Kulthe, S.; Inamdar, N.; Shirolikar, S. Combination of Low and High Molecular Weight Chitosans for the Preparation of Nanoparticles: A Novel Approach Towards Sustained Drug Delivery. Journal of Nanopharmaceutics and Drug Delivery, 2014, 1, 1-12.
79. Dietrich, A.; Neubrand, A. Effects of Particle Size and Molecular Weight of Polyethylenimine on Properties of Nanoparticulate Silicon Dispersions. Journal of the American Ceramic Society, 2001, 84, 806-812.